


ORIGINAL RESEARCH OPEN ACCESS

Computer-Aided Volumetric Quantification of Pre- and Post-Treatment Intracranial Aneurysms in MRA

Subhash Chandra Pal¹ | Chirag Kamal Ahuja² | Dimitrios Toumpanakis³ | Johan Wikstrom³ | Robin Strand⁴  | Ashis Kumar Dhara¹

¹Department of Electrical Engineering, National Institute of Technology, Durgapur, India | ²Department of Radio Diagnosis and Imaging, PGIMER, Chandigarh, India | ³Department of Surgical Sciences, Uppsala University, Uppsala, Sweden | ⁴Department of Information Technology, Uppsala University, Uppsala, Sweden

Correspondence: Robin Strand (robin.strand@it.uu.se)

Received: 19 December 2024 | **Revised:** 11 August 2025 | **Accepted:** 24 August 2025

Funding: This work was supported by the Department of Biotechnology (DBT), Government of India (No. BT/PR41121/Swdn/135/7/2020), and Vinnova, the Swedish Innovation Agency (No. 2020-03616), Government of Sweden.

ABSTRACT

Intracranial aneurysm, a cerebrovascular condition involving abnormal arterial dilation, poses a high risk of subarachnoid hemorrhage upon rupture. Accurate quantification is crucial for diagnosis and follow-up treatment. This paper introduces a novel multi-scale dual-attention network (MSDA-Net) for quantification of intracranial aneurysms in MRA images. The proposed framework includes a context aware patch (CAP) module, multi-scale convolutional blocks, and a dual-attention block, where the CAP module extracts center-line patches to address foreground-background imbalance, the multi-scale and dual-attention blocks enable feature extraction of anatomical dependencies for fine-grained segmentation. The framework leverages three morphological features such as locations of aneurysms, vascular bifurcations, and vessel topology using a multi-task learning scheme for better segmentation. MSDA-Net surpasses state-of-the-art models such as U-Net, residual U-Net, attention U-Net, and nnU-net with an improved dice similarity coefficient of 0.71 and a volume similarity of 0.85. Experiments conducted on the publicly available ADAM challenge dataset and a private post-treatment database demonstrate the reliability and performance of this approach. The method could be used in clinical decision-making in aneurysm follow-up and has profound potential for integration into clinical workflows.

1 | Introduction

Intracranial aneurysm (IA) is a serious cerebrovascular condition with a prevalence of about 6% in the general population, posing significant health risks [1, 2]. When an IA ruptures, it can lead to a subarachnoid hemorrhage, a life-threatening emergency requiring immediate medical intervention. The standard method to prevent rupture is surgical clipping of the aneurysm's neck [3]. However, determining the precise position and orientation for the clip is highly dependent on the surgeon's expertise, making the process both time-consuming and complex.

1.1 | Previous Work

Traditional IAs segmentation techniques relied on manual selection of domain-specific features, which were then used in models for classification, detection, or segmentation tasks. Methods that have been developed for IA segmentation, includes techniques based on filter enhancement [4], region-growing [5], centroid-radii model [6], and blob enhancement [7]. While these methods have shown reasonable performance, they are constrained by the reliance on hand-crafted features derived from prior knowledge and the need for extensive parameter tuning. Recent advances in

This is an open access article under the terms of the [Creative Commons Attribution](https://creativecommons.org/licenses/by/4.0/) License, which permits use, distribution and reproduction in any medium, provided the original work is properly cited.

© 2025 The Author(s). *IET Image Processing* published by John Wiley & Sons Ltd on behalf of The Institution of Engineering and Technology.

deep learning have shown promise in improving the classification and segmentation of IAs, potentially enhancing the accuracy and speed of diagnosis and treatment. However, most current methods rely on two-dimensional (2D) imaging techniques like magnetic resonance imaging (MRI) and computed tomographic angiography (CTA), which lack the ability to fully capture the three-dimensional (3D) structure of the aneurysm [8–10].

Convolutional neural networks (CNNs) like [11, 12] U-Net and ResNet, and particularly 3D models such as DResUNet [13], are commonly applied for aneurysm segmentation in MRA and CTA images, respectively. These architectures, through contracting and expanding pathways with skip connections, capture complex anatomical details efficiently. Pre-processing steps such as voxel resampling, intensity normalization, and skull stripping are crucial for improving image quality, as illustrated in frameworks like the U-Net-based model developed by Stember et al. [14] for cerebral aneurysm segmentation in Time-of-Flight MRA. Further refinements in deep learning architectures address specific challenges, such as enhancing small lesion detection and reducing false positives. For instance, approaches by Claux et al. [15] and Di Noto et al. [16] utilize two-stage U-Nets and probabilistic vessel atlases to boost segmentation precision. Traditional methods often neglected 3D structural intricacies like bifurcation points and connectivity, but recent work emphasizes these elements to enhance segmentation accuracy [17]. In contrast, 3D imaging data offers a more comprehensive understanding of an aneurysm's shape and size, allowing for more accurate diagnosis and more precise treatment planning.

To expedite the interpretation of magnetic resonance angiography (MRA) sequences [18, 19], technicians frequently employ the maximum intensity projection (MIP) [20] technique, which simplifies visualization. However, this method is susceptible to noise and may result in small aneurysms being missed [21]. Therefore, there is an increasing demand for computer-aided detection (CAD) systems to improve the accuracy and effectiveness of aneurysm detection and prevention. These systems can assist clinicians in interpreting time-of-flight MRA (TOF-MRA) volumes, thereby reducing their workload and enhancing the efficiency of clinical diagnosis.

Given these limitations, there is a growing need for CAD systems in clinical practice. CAD systems can enhance the accuracy and efficiency of aneurysm detection by aiding clinicians in interpreting TOF-MRA volumes, thereby reducing their workload and improving diagnostic performance. These systems employ advanced algorithms to analyze the intricate structures within the MRA images, identifying potential aneurysms more reliably than manual methods. Implementing CAD in routine clinical workflows can remarkably improve the early detection and management of intracranial aneurysms.

1.2 | Our Contribution

Most deep learning-based approaches for medical image segmentation are based on the U-Net architecture and its variants [22–25]. Although these models are effective for general segmentation tasks, they face challenges when applied to aneurysm segmen-

TABLE 1 | Ratio of foreground to background(F/B) of randomly selected five subjects from post-treatment dataset original and after pre-processing.

Sl.No.	Original F/B $\times 10^{-5}$	Processed F/B $\times 10^{-5}$
1.	14.10	51.40
2.	1.83	4.77
3.	6.23	72.8
4.	2.76	11.50
5.	0.83	1.91

tation due to the specific complexities of the task and severe class imbalance as shown in Figure 1.

To address the identified challenges, in our previous work, we developed an anatomy-based pre-processing framework [26] that incorporates the anatomical relationship between aneurysm locations and the topology of major cerebral vessels for detailed segmentation. Our approach involved meticulously annotating the major cerebral vessels within MRI scans to precisely localize areas where aneurysms are likely to occur. To achieve this, we identified the maximal area encompassing the annotated vessels and generated a bounding box that accurately encapsulated the vessel structures with minimal inclusion of irrelevant regions. Using this bounding box as a guide, we performed precise cropping of both the original input MRI volume and the corresponding aneurysm mask volume. This step ensured that the cropped images contained all relevant anatomical structures, focusing specifically on areas of potential pathology while eliminating extraneous background. However, our previous framework had two main limitations: (1) Small F/B ratio: the aneurysm region is comparatively smaller to the background, resulting in a heavily imbalanced dataset as shown in Table 1. (2) The performance evaluation indicates suboptimal accuracy in aneurysm segmentation using deep learning methods. To overcome these limitations, we extended our framework by introducing a multi-scale dual attention network (MSDA-Net) incorporating the intrinsic connections between major cerebral vessels and the location of aneurysms. Additionally, we validated the effectiveness of our enhanced framework through extensive analysis and performance evaluation on a pre-and-post treatment IAs database, performing an in-depth analysis and comparison with SOTA networks both quantitatively and qualitatively. The main contribution of the study can be summarized as follows:

1. Annotation of major cerebral vessels of brain MRA images in the context of aneurysm segmentation is for two datasets.
2. A CAP extraction module is proposed for centerline guided patch extraction considering the morphology of major cerebral vessels.
3. The novelty of MSDA-Net lies in its integration of topology-aware multi-scale feature extraction with attention module, enabling precise capture of complex intracranial aneurysm structures. This approach enhances segmentation accuracy and supports improved diagnosis and treatment planning.
4. Extensive experiments indicate that our framework outperforms state-of-the-art methods on the ADAM challenge

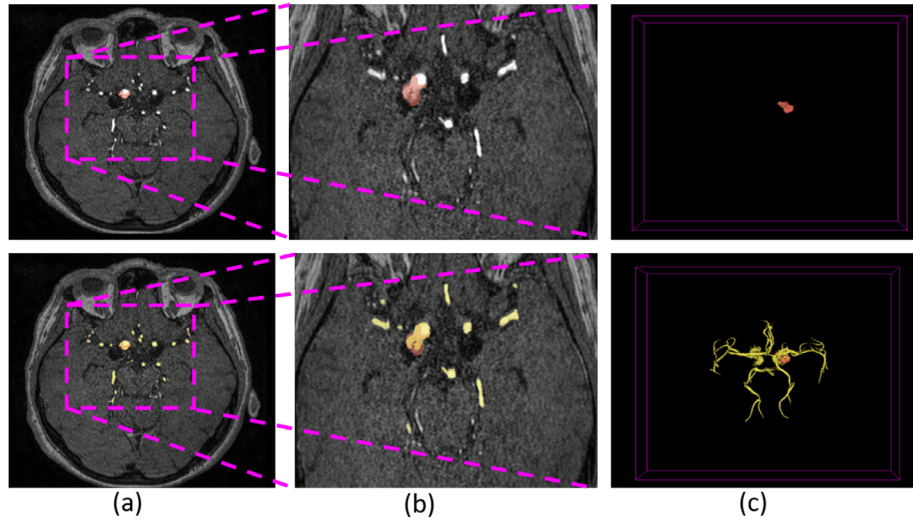


FIGURE 1 | The challenges of accurate IA segmentation. (a),(b) Small volume ratio: the ratio between the aneurysm region and background is highly imbalanced; (c) complex anatomical location: aneurysms are located at junctions or bifurcations of the major cerebral vessels. Where aneurysms and cerebral vessels are marked with red and yellow, respectively.

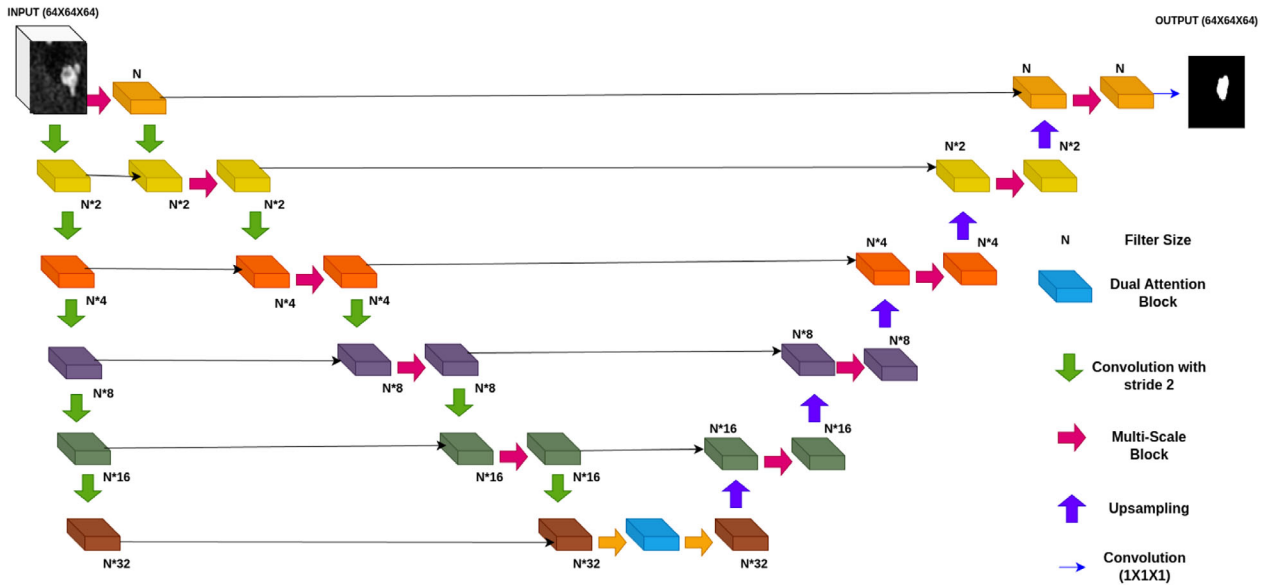


FIGURE 2 | Overview of the proposed MSDA-Net framework. It consists of two blocks: (1) multi-scale block for reducing the semantic gap and (2) dual attention block for channel and spatial attention to capture fine grain topological features.

dataset and our in-house aneurysm remnant database, demonstrating its superior effectiveness.

2 | Methods

In this section, we describe the proposed framework for addressing the task of pre- and post-treatment IA segmentations.

2.1 | Model Architecture

Our proposed architecture as illustrated in Figure 2 follows the encoder-decoder structure of the U-Net [11] with three notable modifications.

First, in place of the standard pair of $3 \times 3 \times 3$ convolutional blocks typically used in U-Net [11], we introduce a novel multi-scale block at each stage except at the bottleneck. This block is designed to capture more detailed features at each level, although it may reduce some finer low-level details. The specific components and functioning of the multi-scale block are explained in detail later. For the final downsampling layer, we employ residual blocks.

Second, to mitigate the loss of fine details caused by the new block, we implement an auxiliary downscaling layer that omits convolutional processing. The output from this auxiliary layer at each step is combined with the corresponding main downscaling layer output through addition. This downscaling uses $2 \times 2 \times 2$ convolutions with a stride of 2, which allows the model to learn

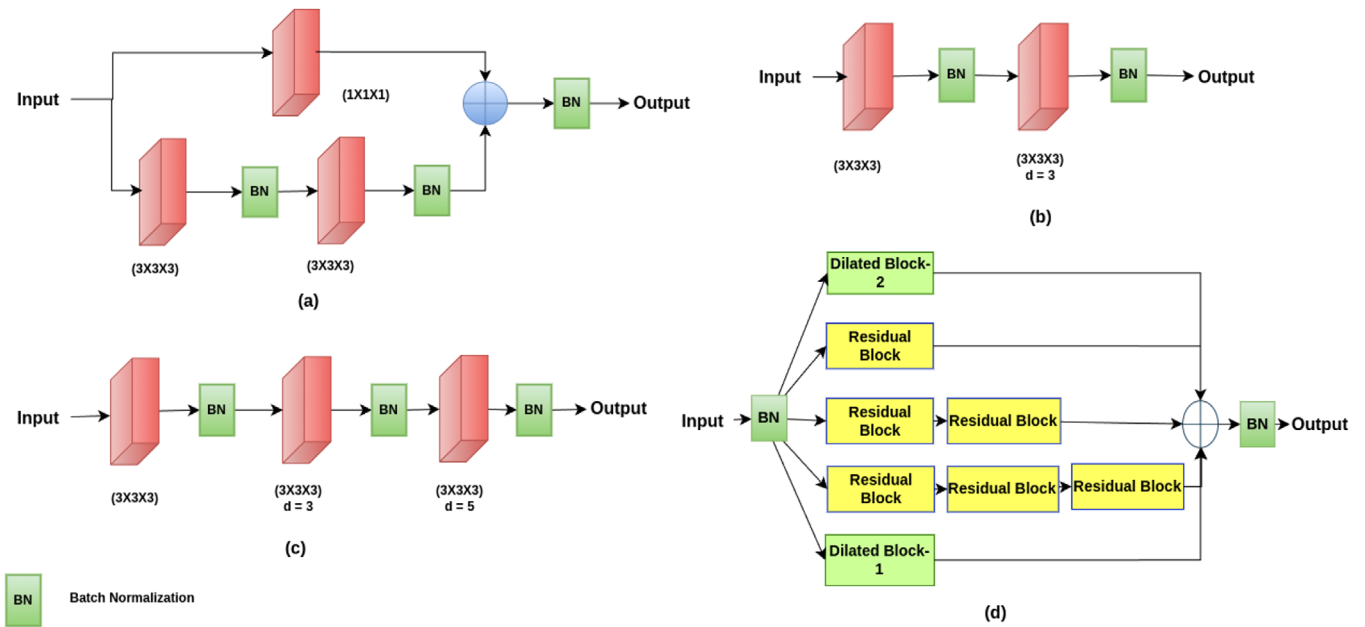


FIGURE 3 | Illustration of different convolutional blocks used in MS block. (a) residual block, (b) dilated block-1, (c) dilated block-2, and (d)MS block.

and retain critical information more effectively than traditional max pooling.

Finally, we employ addition instead of concatenation when merging outputs, following a similar approach to LinkNet [27]. This strategy reduces memory usage and computational demands while delivering improved results. Consequently, the upscaling path requires only half the parameters to match the output size of the downscaling path. We discuss the modifications as follows:

2.1.1 | Multi-Scale Block

Multi-scale block Figure 3 is a novel convolutional block that integrates multiple types of blocks operating in parallel, allowing the network to select the most effective approach at each step. This block ensembles a diverse range of kernel sizes in three different ways, enabling the network to balance the strengths and weaknesses of each block. This diversity in kernel sizes helps the model to accurately identify both the broader regions of interest and the finer edges of the aneurysm structures.

The block also utilizes a one-two-three combination of residual blocks F_2 , F_3 and F_4 based on empirical findings that showed no substantial performance benefits from adding multiple instances of dilated blocks. The additional computational cost was not justified by the minimal gains in accuracy. In this MS block, convolutions with different dilation rates are employed, which allows the network to extract information from varying receptive fields without increasing the number of parameters. Consider the following set of convolutions: a standard $3 \times 3 \times 3$ convolution, a dilated convolution with a dilation rate of 3, and another with a dilation rate of 3, 5. These operations are performed in parallel, and their outputs are concatenated to form a more comprehensive feature map. Mathematically, let the input feature

map be denoted as

$$X \in \mathbb{R}^{C \times D \times H \times W} \quad (1)$$

where C , D , H , and W represent the number of channels, depth, height, and width of the input, respectively.

The feature maps F_1 and F_5 generated by convolutions with different dilation rates d_1 and d_2 can be expressed as:

$$F_1 = \text{Conv}(X, W_1, d_1). \quad (2)$$

$$F_5 = \text{Conv}(X, W_2, d_2), \quad (3)$$

where W_1 and W_2 are the learned weights for each convolution operation. These convolutions capture local and global information by adjusting the dilation rates d , with $d_1 = 3$ and $d_2 = 5$ for the dilated convolutions.

The outputs of these convolution operations are concatenated with the residual blocks, which ensures that the original information is preserved while enhancing feature representation. Let the concatenated feature map be F as:

$$F = [F_1; F_2; F_3; F_4; F_5]. \quad (4)$$

This process enables the MS block to encode features from multiple scales, allowing it to handle complex structures like aneurysms, which can manifest in various shapes and sizes across different slices of medical scans. By integrating multi-scale information, the MS block enhances the segmentation network's ability to accurately segment fine details as well as larger structures, improving overall performance in tasks such as aneurysm segmentation.

2.1.2 | Dual-Attention Block

The dual attention mechanism integrates both channel and spatial attention to improve feature representation for segmentation tasks [26]. In aneurysm segmentation, this is particularly valuable as it helps model complex geometrical structures that require both local and global context. The Spatial Attention module operates on local feature maps $I \in \mathbb{R}^{C \times D \times H \times W}$. These feature maps are first processed through 1x1x1 convolution layers to generate three intermediate feature maps, denoted as A , B , and C , where $\{A, B, C\} \in \mathbb{R}^{C \times D \times H \times W}$. The feature maps are then reshaped into vectors A' , B' , and $C' \in \mathbb{R}^{C \times N}$, where $N = D \times H \times W$ represents the total number of voxels. A spatial attention map $S \in \mathbb{R}^{N \times N}$ is generated by applying a softmax function to the matrix product of the transpose of A' and B' :

$$s_{j,i} = \frac{\exp((A')_i^T \cdot B_j)}{\sum_{i=1}^N \exp((A')_i^T \cdot B_j)} \quad (5)$$

The value $s_{j,i}$ quantifies the impact of the i^{th} voxel on the j^{th} voxel, with higher values indicating stronger correlations. This spatial attention map is then multiplied with C' , and the result is reshaped back to $\mathbb{R}^{C \times D \times H \times W}$, followed by an element-wise summation to enhance the spatial context.

The channel attention module, uses the original feature map $X \in \mathbb{R}^{C \times D \times H \times W}$ to model interdependencies among channels. By generating a channel attention map, this module adjusts the significance of different channels based on their relevance to the segmentation task. Each channel's feature is recalculated as a weighted sum of all channel features, enhancing the model's understanding of long-range dependencies. The spatial attention map, meanwhile, provides a broader contextual perspective, highlighting prominent anatomical regions of interest. The outputs from both attention mechanisms are aggregated to produce refined features, improving the segmentation performance for aneurysm detection and quantification.

In addition to channel attention, spatial attention captures the spatial context by highlighting the most critical regions in the feature space. This selective focus enables the network to incorporate more diverse contextual information, enriching the local feature representation and improving intra-class consistency. The combination of spatial and channel attention refines feature extraction, leading to more precise and accurate segmentation of aneurysms.

3 | Experiments

This section describes the dataset both public and in-house, the experimental setup for training and inferencing, and the evaluation metrics.

3.1 | Dataset

3.1.1 | Public

This study conducts a comparative analysis of the performance of existing deep learning models on the publicly available Aneurysm

TABLE 2 | Dataset split form public and private dataset for pre-and post-treatment.

Category	Type	No. of volumes
Public dataset (ADAM challenge)	Pre-treatment (distinct/baseline)	78
Public dataset (ADAM challenge)	Post-treatment (follow-up)	35
Private dataset	Post-treatment (no follow-up available)	36

Detection And segMentation (ADAM) dataset [28] and a private dataset obtained from Uppsala University Hospital, Sweden as shown in Table 2. The dataset comprises 3D TOF-MRA images, with a total of 113 cases. Out of these, 93 volumes contain at least one untreated, unruptured aneurysm, including 35 pre-treatment (baseline) volumes and 35 post-treatment (follow-up) volumes from the same subjects, along with 23 volumes from distinct individuals whose treatment status is not explicitly specified. Additionally, 20 volumes are included that do not show any intracranial aneurysms. We consider both distinct and no intracranial aneurysm volumes as pre-treatment volumes.

The median age of the 53 subjects with unruptured intracranial aneurysms was 55 years, and 75% of them were female. To correct intensity non-uniformities in the images, the N4 bias correction algorithm was applied, effectively mitigating low-frequency intensity variations [29]. In the aneurysm label images, the background is indicated by 0, untreated and unruptured aneurysms are labeled as 1, and treated aneurysms or artifacts from treatments are labeled as 2. Given that the main goal of this study is to segment pre- and post-treatment aneurysms automatically, label 2 is excluded from the evaluation process.

3.1.2 | Private

The dataset utilized in this study comprises post-treatment MR scans from a total of 42 subjects from Uppsala University Hospitals, Sweden (approved by the local ethics committee as part of a prospective research study). Among them, 36 subjects exhibit remnants of treated intracranial aneurysms (post-treatment cases), while the remaining subjects show no remnants. These scans were obtained using MR Phillips Medical Systems, and to comply with clinical standards, all relevant patient information was anonymized from the DICOM header files. The imaging data for this study was acquired using a 3T MRI scanner, with specific parameters tailored for optimal intracranial aneurysm visualization. The voxel dimensions were set to $0.5 \times 0.7 \times 1 \text{ mm}^3$, ensuring a high-resolution capture of the cerebral anatomy. Each volume consisted of 148 to 150 slices, with a matrix size of 512×512 pixels, providing detailed spatial coverage. The repetition time (TR) and echo time (TE) were 25 ms and 1.7 ms, respectively, while the flip angle was set at 20 degrees. These parameters were carefully chosen to balance image quality and acquisition time, making them ideal for aneurysm analysis in the clinical setting. Annotation of the scans was performed manually using 3D-Slicer

Require: X , Y and V are the MRA image, aneurysm mask and major vessel mask.

- 1: $V_{bin} \leftarrow V > 0$ ▷ Binarize to foreground and background labels
- 2: $V_{skel} \leftarrow \text{skeletonize}(V_{bin})$ ▷ Extract binarized skeleton
- 3: $V_{skel} \leftarrow \text{location}(V_{i,j,k})$ ▷ Centerline coordinates (i, j, k)
- 4: $Y_{mask} \leftarrow \text{crop}(Y_{i,j,k})$ ▷ Crop at center coordinates (i, j, k)
- 5: $X_{image} \leftarrow \text{crop}(X_{i,j,k})$ ▷ Crop at center coordinates (i, j, k)
- 6: **return** Y_{mask} and X_{image}

[30] software by members of our expert team. One annotator focused on marking the cerebral vasculature, while another identified the location of the intracranial aneurysm remnants. Subsequently, a domain expert in neuroradiology with over 25 years of experience verified these annotations. Any discrepancies were resolved through consensus among the three experts on the team.

3.2 | Experimental Setup and Training

Intracranial aneurysms can occur at various locations within the cerebral vasculature, with some regions being more commonly affected, such as the Circle of Willis and other major cerebral vessels. Context-aware patch module is proposed to effectively capture relevant features along the vessel skeleton in MRA images, standardized 3D patches were extracted. This extraction process involved precise vessel skeletonization techniques, including thresholding, binary conversion, and region-growing algorithms to define the vascular structures accurately as illustrated in Algorithm 1. The patches sized at $(64 \times 64 \times 64)$ voxels, were centered along the vessel centerline and extended evenly from both segmented vessel edges. By sliding a window along the centerline and cropping the image, this approach emphasizes the importance of centerline patch extraction in segmenting post-treatment intracranial aneurysms and analyzing medical images.

An interesting challenge in deep learning-based segmentation is addressing the substantial class imbalance between normal and aneurysm patches in MRA images. To mitigate this, various data augmentation techniques, such as flipping, zooming, noise injection, rotation, blurring, and contrast adjustments, were employed to increase the variability of the training data. These augmentations helped to generate diverse examples, improve the model's ability to detect aneurysms across different imaging conditions, and reduce overfitting, ultimately enhancing the accuracy and reliability of the segmentation outcomes.

The deep learning-based segmentation methods were implemented using TensorFlow on a Dell Precision GPU system. For a thorough evaluation, the dataset is equally divided into training, validation, and test sets. For the public dataset, the split ensures balanced representation of pre-treatment and post-treatment cases. Similarly, as the private dataset only consists of post-treatment cases so we divide them equally across the sets. Additionally, a 3-fold cross-validation is applied to ensure

robust model evaluation and mitigate overfitting. In our experiments, we employed the dice loss function as the primary loss measure. The Dice Similarity Coefficient (DSC) evaluates the degree of overlap between two sets, such as predicted and ground truth segmentations.

The dice loss function is mathematically expressed as:

$$\mathcal{L}_{\text{dice}} = 1 - \frac{2 \sum_{i=1}^N x_i y_i}{\sum_{i=1}^N x_i^2 + \sum_{i=1}^N y_i^2 + \epsilon} \quad (6)$$

Here, x_i represents the predicted voxel value, y_i denotes the ground truth voxel value for i -th sample, and ϵ is a small constant added to the numerator and denominator to prevent division by zero in cases where there may be no overlap. The Adam [31] optimization algorithm was chosen for hyper-parameter optimization, with an initial learning rate set at 0.0001 and decayed using exponential annealing. The TensorBoard callback facilitated the visualization of training metrics, while EarlyStopping was used to halt training when the validation loss did not improve for 10 epochs. For evaluating the metrics, $(64 \times 64 \times 64)$ patches were taken comprising the major brain vessel centerline, then efficiently negative patches were discarded and all the positive patches were considered for evaluation where patches having no aneurysms were negative, and patches with aneurysms were positive.

3.3 | Evaluation Metrics

In this study, we quantitatively analyze the performance of automated methods for segmenting aneurysms by comparing them with manually annotated input volumes (I) and predicted output volumes(O) [32]. Furthermore, we employ the DSC metrics to assess the correlation between automated segmentation and ground truth volumes for each patient. The DSC quantifies similarity between two datasets, with values ranging from 0 to 1; a DSC of 1 indicates perfect agreement between the datasets.

$$\text{DSC} = \frac{2 \times |O_1 \cap I_1|}{|O_1| + |I_1|} \quad (7)$$

Additionally, we utilize volumetric similarity (VS) and the Hausdorff distance (HD) 95th percentile to analyze the shape and structure of aneurysms. VS is a metric in 3D medical image segmentation that measures similarity between segmented and ground truth volumes, ranging from 0 (no similarity) to 1 (perfect similarity).

$$\text{VS} = 1 - \frac{||O_1| - |I_1||}{|O_1| + |I_1|} \quad (8)$$

The Hausdorff distance (HD) is crucial in medical image segmentation for assessing shape similarity, which is pertinent in surgical planning in segmenting post-treatment intracranial aneurysms. HD measures the maximum distance between points in one set to the closest point in another set, providing a measure of spatial dissimilarity between them [33]. It can be computed using Equation 9, where O and I denote segmented and ground truth volumes, respectively, and $d(o,i)$ represents the distance between

TABLE 3 | Quantitative performance measure of different networks on the test-set for ADAM dataset.

3D networks/metrics	DSC (%)	HD(mm)	VS
U-Net [34]	35.24	38.21	0.45
Attention U-Net [12]	40.65	36.75	0.53
Residual U-Net [35]	45.95	33.51	0.58
Residual attention U-Net [36]	49.58	31.95	0.59
nnU-Net [37]	59.27	26.35	0.63
MSDA-Net	61.23	25.35	0.65

TABLE 4 | Quantitative performance measure of different networks on the test-set for post-treatment in-house dataset.

3D networks/metrics	DSC (%)	HD(mm)	VS
U-Net [34]	45.34	40.21	0.62
Attention U-Net [12]	59.35	39.45	0.67
Residual U-Net [35]	56.76	35.41	0.69
Residual attention U-Net [36]	62.53	29.75	0.71
nnU-Net [37]	67.29	18.73	0.79
MSDA-Net	71.60	11.53	0.85

points o and i .

$$HD(O, I) = \max \left\{ \sup_{o \in O} \inf_{i \in I} \|o - i\|, \sup_{i \in I} \inf_{o \in O} \|o - i\| \right\} \quad (9)$$

4 | Results and Discussions

This section highlights the performance analysis of MSDA-Net evaluated on private and publicly available databases. It includes results, discussions and limitations.

4.1 | Results

The results presented in Tables 3 and 4 demonstrate the performance of various deep learning models on the ADAM dataset and post-treatment in-house dataset. The performance metrics include DSC, HD and VS, which provide a comprehensive evaluation of the segmentation models. MSDA-Net consistently outperforms other models across all metrics, showing superior segmentation accuracy and robustness.

In the ADAM dataset (Table 3), MSDA-Net achieved a DSC of 61.23%, considerably higher than the other networks, such as nnU-Net 59.27% and attention U-Net 40.65%. The Hausdorff distance (HD), which measures the largest segmentation error between predicted and ground truth boundaries, was also minimized with MSDA-Net at 25.35, compared to 26.35 for nnU-Net. These results indicate that MSDA-Net not only improves segmentation accuracy but also reduces the boundary mismatch between the predicted aneurysm region and the actual ground truth, leading to more precise clinical diagnoses (Figure 4).

A crucial aspect of result evaluation is understanding the presence of false positives (FP) and false negatives (FN). FP occur

when the model mistakenly identifies a normal region as an aneurysm, while false negatives arise when the model fails to detect an actual aneurysm. In the ADAM dataset, the lower HD in MSDA-Net gives fewer false positives, meaning the model is less likely to incorrectly classify healthy regions as aneurysms. Conversely, a higher DSC implies fewer false negatives, as the model is better at capturing aneurysms with high sensitivity. This reduction in FNs is vital in medical applications because missing a true aneurysm could lead to severe consequences, such as failure to intervene before a rupture.

For the post-treatment in-house dataset (Table 4), MSDA-Net achieved an even higher DSC of 71.60%, reflecting its robustness in handling complex medical data. The notable reduction in HD to 11.53 indicates that MSDA-Net effectively reduces both FP and FN rates (Figure 5). This enhanced accuracy in post-treatment scenarios is crucial, as false positives may lead to unnecessary follow-up procedures, while false negatives could result in undetected aneurysm regrowth or complications after interventions such as coiling or clipping. To further validate the performance difference, we conducted a statistical analysis comparing MSDA-Net and nnU-Net using a paired t-test on the DSC metric for in-house dataset, yielding a p-value of 3.25×10^{-7} . The model's ability to handle these complexities ensures that it can be reliably used in clinical workflows, improving patient outcomes through more accurate and timely treatment assessments.

The quantitative and qualitative results indicate that MSDA-Net offers substantial improvements over traditional medical image segmentation models by minimizing false positives and false negatives, enhancing the overall reliability of segmentation for both initial diagnosis and post-treatment follow-up of intracranial aneurysms. This demonstrates the potential of MSDA-Net in automating critical medical processes, reducing the burden on radiologists, and ensuring more accurate patient management.

4.2 | Volumetric Analysis

In our study, volumetric quantification was conducted to analyze aneurysm progression between baseline and follow-up imaging. This evaluation is particularly significant in post-treatment scenarios, we have used the public available baseline and follow-up volumes for assessment. For each subject, volume differences were calculated by comparing aneurysm volumes at baseline and follow-up using both the manual annotations and the MSDA-Net generated segmentations. As shown in Figure 6, the predicted volume differences exhibit strong consistency with the ground truth, reflecting the model's capability to approximate clinically meaningful volume trends across patients. These results affirm that the proposed segmentation framework is not only effective in delineating aneurysm boundaries but also in preserving volumetric integrity across time-points. This characteristic is critical in longitudinal studies, where precise volume estimation plays a central role in clinical decision making and outcome evaluation.

4.3 | Discussions

The proposed MSDA-Net framework demonstrates considerable improvements in the segmentation and quantification of IA, as

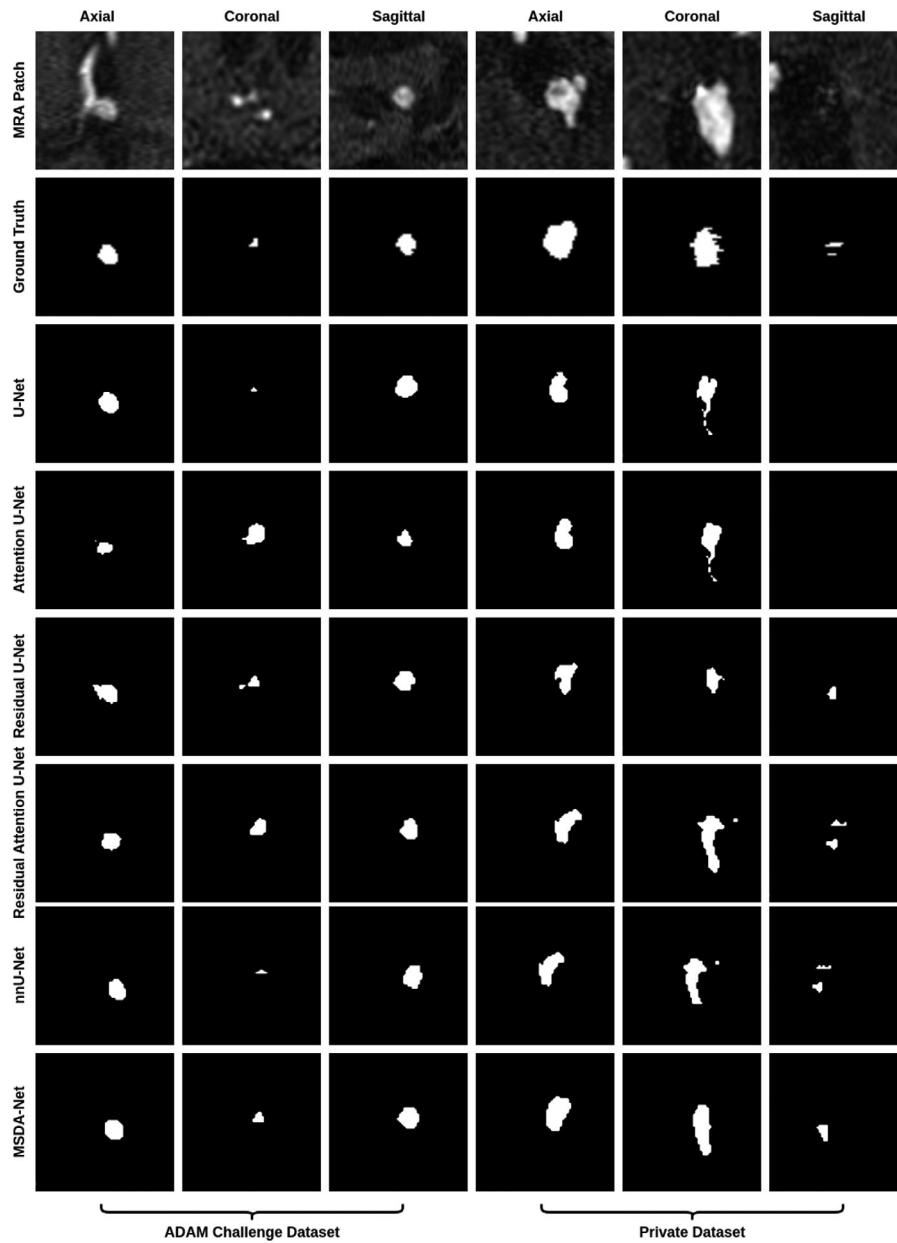


FIGURE 4 | Comparison of segmentation of pre-and post-treatment aneurysms visualization with different deep learning methods and MSDA-Net.

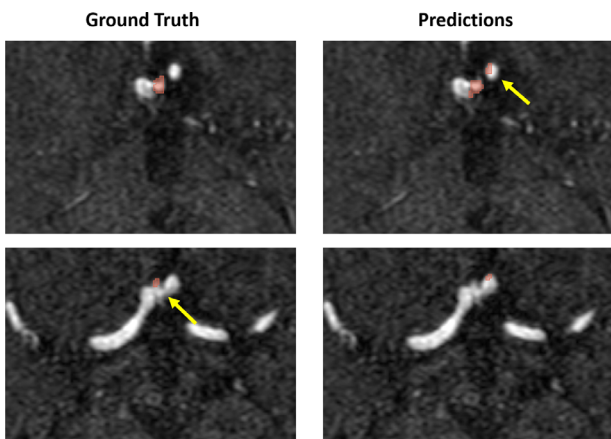


FIGURE 5 | Example of false positive(top) and false negative(bottom) from randomly selected test result.

evidenced by the results on both the ADAM dataset and the post-treatment in-house dataset. One of the key challenges in medical image segmentation, especially in the case of intracranial aneurysms, is the presence of extreme class imbalance between the aneurysm regions and the surrounding normal tissue. The MSDA-Net addresses this by incorporating a pre-processing context-aware patch module, which mitigates the effect of this imbalance and reduces the occurrence of false positives and false negatives. This is particularly valuable in post-treatment monitoring and follow-up studies. By integrating multi-scale attention mechanisms, the model successfully captures contextual anatomical structures, improving the quantification of aneurysms with higher precision. The use of both channel and spatial attention plays a pivotal role in refining feature representations, leading to enhanced segmentation outcomes.

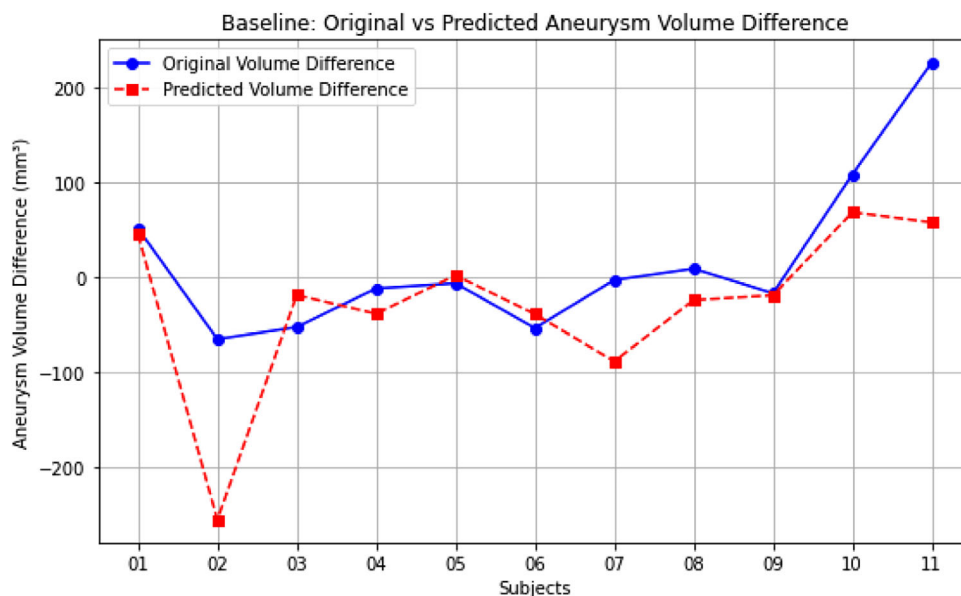


FIGURE 6 | Subject-wise comparison of aneurysm volume differences between baseline and follow-up scans using manual (original) and predicted segmentations. Positive values indicate an increase in aneurysm volume, while negative values indicate a reduction.

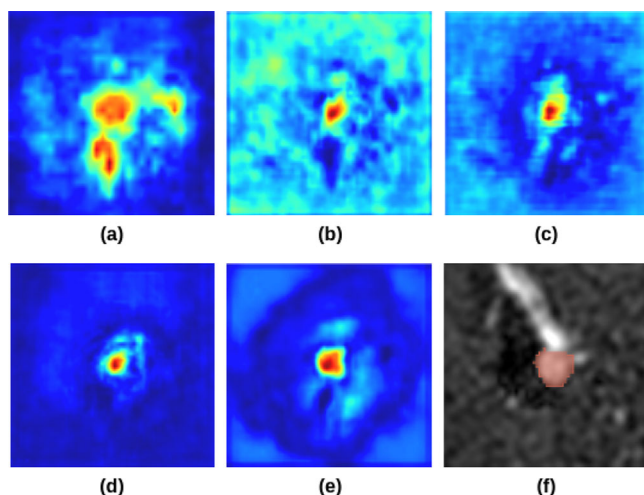


FIGURE 7 | (a)–(e) display the feature maps generated by the different stages of the MSDA-Net, while (f) illustrates the corresponding ground truth from the post-treatment dataset. In the feature maps, areas highlighted in red indicate higher values, whereas areas in blue signify lower values.

The saliency map visualizations generated from different layers of the MSDA-Net as depicted Figure 7 offer critical insights into how the model progressively refines its focus on regions of interest in medical images. As shown in the earlier layers in Figure 3, the activations are more diffuse, reflecting the network's broad scanning of features across the image. This diffuse nature indicates that the network is initially learning to recognize general patterns and structures, though with lower confidence in identifying the precise location of the abnormality. However, as the model advances through deeper layers, the heatmaps show increasingly concentrated activations, demonstrating that the network is honing in on the critical regions, such as potential aneurysm sites, with greater specificity.

By the final layers, the heatmap activations become sharply focused, aligning closely with the areas of true clinical interest. This progression highlights the efficacy of MSDA-Net's multiscale dilated convolutions and attention mechanism in enhancing feature localization and segmentation accuracy. The model's ability to reduce these errors directly contributes to more reliable neuro-interventional surgical planning, offering insights for its integration into real-world clinical settings.

4.4 | Clinical Significance

Deep learning based segmentation and quantification of pre and post-treatment intracranial aneurysms hold substantial clinical importance, particularly in enhancing follow-up treatment and management strategies that involve the critical role of major cerebral vessels. These advanced computational methods provide precise, automated tools for monitoring changes in aneurysm morphology over time, which is vital for evaluating the effectiveness of treatments and predicting patient outcomes. By accurately segmenting aneurysms and quantifying their key characteristics such as size, shape, and their spatial relationship with major cerebral vessels clinicians can more effectively track the progression of aneurysms and assess their response to interventions like coiling or clipping.

Integrating deep learning algorithms with anatomical knowledge of cerebral vessels enables a more detailed analysis of the complex morphological features of aneurysms, thereby improving diagnostic accuracy and supporting better clinical decision-making. This approach helps in identifying potential post-treatment complications, such as aneurysm recurrence or residual growth, which could prominently affect patient prognosis. Additionally, these techniques allow for the efficient processing of large volumes of imaging data, reducing the workload on radiologists and optimizing clinical workflows. Ultimately, by offering a comprehensive understanding of post-treatment aneurysm dynamics

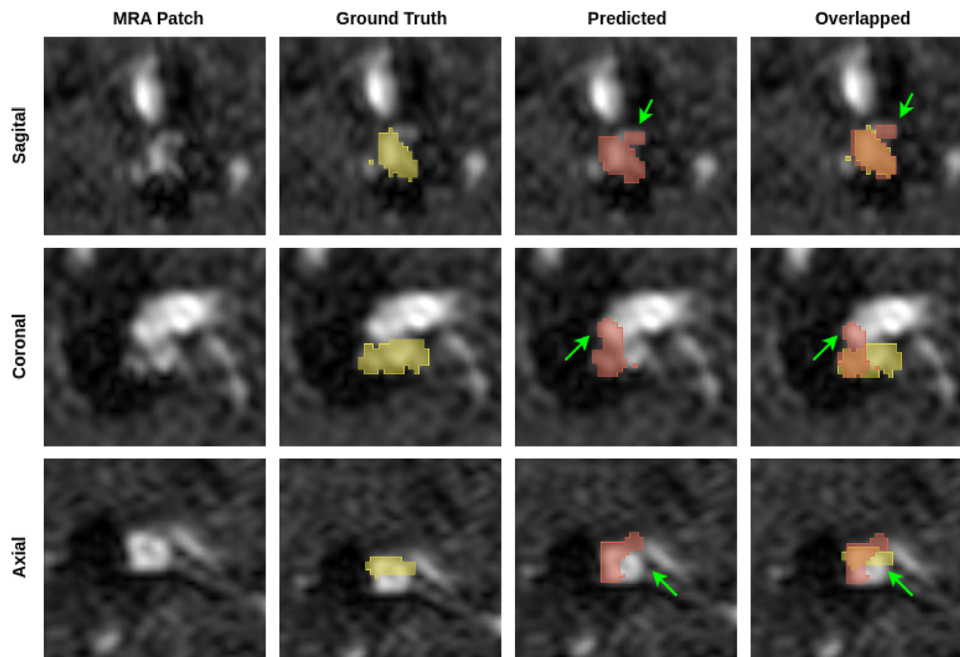


FIGURE 8 | Qualitative assessment of segmentation results generated using the MSDA-Net on a low performing randomly chosen subjects. The yellow, red colour indicates ground truth and predicted regions, respectively. The green arrow indicates the misclassified voxels.

and their interactions with critical cerebral vessels, deep learning based segmentation enhances personalized treatment planning and contributes to improved long term care for patients with neurovascular conditions.

4.5 | Limitations

The proposed approach has certain limitations, as the network encounters challenges in accurately analyzing some test subjects. Figure 8 shows the axial, coronal, and sagittal views of a sample with lower performance. Due to the complex geometry of aneurysms, the network sometimes struggles to distinguish intricate vascular structures and aneurysms effectively. Additionally, the grayscale values of aneurysm remnants often resemble nearby veins or other vessel branches, which can lead to misinterpretation. Artifacts such as calcifications and surgical clips may appear similar to aneurysm remnants, resulting in potential false positives and over-segmentation. Moreover, inconsistencies in labeling practices across different centers introduce data discrepancies, which could be mitigated by developing methods to handle label noise and incomplete labeling. The private dataset currently consists solely of post-treatment data without follow-up imaging, limiting the ability to perform volumetric trend analysis. Another limitation is the generalizability of MSDA-Net to images acquired from different MRI scanners and protocols. The private dataset was obtained using a single MRI scanner and a consistent imaging protocol, ensuring uniformity during the evaluation. While this setup allowed for a controlled performance assessment, it restricts the model's applicability to data from other scanners or protocols. Additionally, the public dataset used in this study lacks detailed information about the specific scanners and imaging parameters, preventing a comprehensive evaluation of the model's cross-scanner generalizability. In the future, our work will focus on addressing these challenges to enhance intracranial

aneurysm quantification also we plan to enhance the dataset by incorporating follow-up data, enabling more comprehensive longitudinal studies.

5 | Conclusion

This research presents MSDA-Net to precisely segment and quantify intracranial aneurysms from MRA images. By incorporating context-aware patch extraction and multi-scale dual-attention modules, the model effectively captures the complex morphological features of aneurysms while addressing class imbalance and background noise challenges. The experimental results on both public and private datasets highlight its better performance over existing approaches, demonstrating notable improvements in segmentation accuracy and reduction of false predictions. Overlapping anatomical structures and poor image contrast impose limitations on acceptable segmentation of small aneurysms. Future research aims to enhance the framework's generalizability and robustness on broader datasets. The proposed network could be used for developing tools for automated diagnosis and treatment response quantification.

Author Contributions

Subhash Chandra Pal contributed to the conceptualization, formal analysis, investigation, methodology, software development, validation, visualization, and preparation of the original draft. **Chirag Kamal Ahuja, Dimitrios Toumpanakis** and **Johan Wikstrom** contributed to data curation, validation, and visualization. **Robin Strand** oversaw formal analysis, funding acquisition, investigation, project administration, and resource allocation while contributing to validation and the review and editing of the manuscript. **Ashis Kumar Dhara** provided support in formal analysis, funding acquisition, investigation, project management, validation, and manuscript review and editing.

Acknowledgements

The authors gratefully acknowledge the support provided by the Department of Biotechnology (DBT), Government of India (No. BT/PR41121/Swdn/135/7/2020), and Vinnova, the Swedish Innovation Agency (No. 2020-03616), Government of Sweden, for this work.

Conflicts of Interest

The authors declare no potential conflict of interests.

Data Availability Statement

The Aneurysm Detection and Segmentation (ADAM) dataset is a public dataset and can be downloaded from <https://adam.isi.uu.nl/data/>. The Uppsala University post-treatment aneurysm dataset is private and may be available upon request to the corresponding author.

References

1. M. H. Vlak, A. Algra, R. Brandenburg, and G. J. Rinkel, "Prevalence of Unruptured Intracranial Aneurysms, With Emphasis on Sex, age, Comorbidity, Country, and Time Period: a Systematic Review and Meta-Analysis," *The Lancet Neurology* 10, no. 7 (2011): 626–636.
2. A. Vaswani, "Attention is All You Need," in *Advances in Neural Information Processing Systems* (Curran Associates, Inc., 2017).
3. S. D'Souza, "Aneurysmal Subarachnoid Hemorrhage," *Journal of Neurosurgical Anesthesiology* 27, no. 3 (2015): 222–240.
4. T. Jerman, F. Pernuš, B. Likar, and Ž. Špiclin, "Blob Enhancement and Visualization for Improved Intracranial Aneurysm Detection," *IEEE Transactions on Visualization and Computer Graphics* 22, no. 6 (2015): 1705–1717.
5. R. Adams and L. Bischof, "Seeded Region Growing," *IEEE Transactions on Pattern Analysis and Machine Intelligence* 16, no. 6 (1994): 641–647.
6. A. Lauric, E. L. Miller, M. I. Baharoglu, and A. M. Malek, "Rupture Status Discrimination in Intracranial Aneurysms Using the Centroid-Radii Model," *IEEE Transactions on Biomedical Engineering* 58, no. 10 (2011): 2895–2903.
7. R. Shahzad, L. Pennig, L. Goertz, F. Thiele, C. Kabbasch, M. Schlamann, B. Krischek, D. Maintz, M. Perkuhn, and J. Borggrefe, "Fully Automated Detection and Segmentation of Intracranial Aneurysms in Subarachnoid Hemorrhage on CTA Using Deep Learning," *Scientific Reports* 10, no. 1 (2020): 21799.
8. R. D. Brown and J. P. Broderick, "Unruptured Intracranial Aneurysms: Epidemiology, Natural History, Management Options, and Familial Screening," *The Lancet Neurology* 13, no. 4 (2014): 393–404.
9. J. P. Broderick, C. M. Viscoli, T. Brott, W. N. Kernan, L. M. Brass, E. Feldmann, L. B. Morgenstern, J. L. Wilterdink, and R. I. Horwitz, "Major Risk Factors for Aneurysmal Subarachnoid Hemorrhage in the Young are Modifiable," *Stroke* 34, no. 6 (2003): 1375–1381.
10. C. Y. Chung, R. B. Peterson, B. M. Howard, and M. E. Zygmunt, "Imaging Intracranial Aneurysms in the Endovascular Era: Surveillance and Posttreatment Follow-Up," *RadioGraphics* 42, no. 3 (2022): 789–805.
11. N. Siddique, S. Paheding, C. P. Elkin, and V. Devabhaktuni, "U-Net and Its Variants for Medical Image Segmentation: A Review of Theory and Applications," *IEEE Access* 9 (2021): 82031–82057.
12. O. Oktay, J. Schlemper, L. L. Folgoc, M. Lee, M. Heinrich, K. Misawa, K. Mori, S. McDonagh, N. Y. Hammerla, B. Kainz, et al., "Attention U-Net: Learning Where to Look for the Pancreas," arXiv preprint, arXiv:1804.03999 (2018).
13. S. M. Smith, "Fast Robust Automated Brain Extraction," *Human Brain Mapping* 17, no. 3 (2002): 143–155.
14. T. Sichter, A. Faron, R. Sijben, N. Teichert, J. Freiherr, and M. Wiesmann, "Deep Learning-Based Detection of Intracranial Aneurysms in 3D TOF-MRA," *American Journal of Neuroradiology* 40, no. 1 (2019): 25–32.
15. F. Claux, M. Baudouin, C. Bogey, and A. Rouchaud, "Dense, Deep Learning-Based Intracranial Aneurysm Detection on TOF MRI Using Two-Stage Regularized U-Net," *Journal of Neuroradiology* 50, no. 1 (2023): 9–15.
16. T. Di Noto, G. Marie, S. Tourbier, Y. Alemán-Gómez, O. Esteban, G. Saliou, M. B. Cuadra, P. Hagmann, and J. Richiardi, "Towards Automated Brain Aneurysm Detection in TOF-MRA: Open Data, Weak Labels, and Anatomical Knowledge," *Neuroinformatics* 21, no. 1 (2023): 21–34.
17. W. Xu, C. Li, Y. Bian, Q. Meng, W. Zhu, F. Shi, X. Chen, C. Shao, and D. Xiang, "Cross-Modal Consistency for Single-Modal MR Image Segmentation," *IEEE Transactions on Biomedical Engineering* 71, no. 9 (2024): 2557–2567.
18. S. C. Pal, S. Banerjee, D. Toumpanakis, J. Wikström, R. Strand, and A. K. Dhara, "Segmentation of Major Cerebral Vessel from MRA Images and Evaluation Using U-Net Family," in *2022 IEEE 6th International Conference on Condition Assessment Techniques in Electrical Systems (CATCON)* (IEEE, 2022), pp. 235–238.
19. P.-y. Teng, A. M. Bagci, and N. Alperin, "Automated Prescription of an Optimal Imaging Plane for Measurement of Cerebral Blood Flow by Phase Contrast Magnetic Resonance Imaging," *IEEE Transactions on Biomedical Engineering* 58, no. 9 (2011): 2566–2573.
20. Ö. Çiçek, A. Abdulkadir, S. S. Lienkamp, T. Brox, and O. Ronneberger, "3d U-Net: Learning Dense Volumetric Segmentation from Sparse Annotation," in *Medical Image Computing and Computer-Assisted Intervention – MICCAI 2016: 19th International Conference, Athens, Greece, October 17–21, 2016, Proceedings, Part II 19* (Springer, 2016), 424–432.
21. A. M. Sailer, B. A. Wagemans, P. J. Nelemans, R. de Graaf, and W. H. van Zwam, "Diagnosing Intracranial Aneurysms With MR Angiography: Systematic Review and Meta-Analysis," *Stroke* 45, no. 1 (2014): 119–126.
22. A. Firouzian, R. Manniesing, Z. H. Flach, et al., "Intracranial Aneurysm Segmentation in 3D CT Angiography: Method and Quantitative Validation With and Without Prior Noise Filtering," *European Journal of Radiology* 79, no. 2 (2011): 299–304.
23. S. Wang, L. Li, H. Gao, K. Zhang, Q.-J. Shao, T. Li, and B. Gao, "Middle Cerebral Artery Bifurcation Aneurysms are Associated With Patient Age, Sex, Bifurcation Angle, and Vascular Diameters," *Scientific Reports* 13, no. 1 (2023): 22844.
24. J. Zhang, A. Can, P. M. R. Lai, et al., "Morphological Variables Associated With Ruptured Basilar Tip Aneurysms," *Scientific Reports* 11, no. 1 (2021): 2526.
25. J. Li, Z. L. Yu, Z. Gu, H. Liu, and Y. Li, "Dilated-Inception Net: Multi-scale Feature Aggregation for Cardiac Right Ventricle Segmentation," *IEEE Transactions on Biomedical Engineering* 66, no. 12 (2019): 3499–3508.
26. S. C. Pal, D. Toumpanakis, J. Wikström, C. K. Ahuja, R. Strand, and A. K. Dhara, "Multi-Level Residual Dual Attention Network for Major Cerebral Arteries Segmentation in MRA towards Diagnosis of Cerebrovascular Disorders," *IEEE Transactions on NanoBioscience* 23, no. 1 (2024): 167–175.
27. A. Chaurasia and E. Cukurciello, "Linknet: Exploiting Encoder Representations for Efficient Semantic Segmentation," in *2017 IEEE Visual Communications and Image Processing (VCIP)* (IEEE, 2017), 1–4.
28. K. M. Timmins, I. C. van der Schaaf, E. Bennink, et al., "Comparing Methods of Detecting and Segmenting Unruptured Intracranial Aneurysms on TOF-MRAs: The Adam Challenge," *Neuroimage* 238 (2021): 118216.
29. N. J. Tustison, B. B. Avants, P. A. Cook, et al., "N4itk: Improved n3 Bias Correction," *IEEE Transactions on Medical Imaging* 29, no. 6 (2010): 1310–1320.
30. S. Pieper, M. Halle, and R. Kikinis, "3D Slicer," in *2004 2nd IEEE International Symposium on Biomedical Imaging: Nano to Macro (IEEE Cat No. 04EX821)* (IEEE, 2004), 632–635.

31. D. P. Kingma, "Adam: A Method for Stochastic Optimization," arXiv preprint, arXiv:1412.6980 (2014).
32. A. A. Taha and A. Hanbury, "Metrics for Evaluating 3D Medical Image Segmentation: Analysis, Selection, and Tool," *BMC Medical Imaging* 15 (2015): 1–28.
33. M.-P. Dubuisson and A. K. Jain, "A Modified Hausdorff Distance for Object Matching," in *Proceedings of 12th International Conference on Pattern Recognition*, Vol. 1 (IEEE, 1994), 566–568.
34. O. Ronneberger, P. Fischer, and T. Brox, "U-net: Convolutional Networks for Biomedical Image Segmentation," in *Medical image computing and computer-assisted intervention–MICCAI 2015: 18th international conference, Munich, Germany, October 5–9, 2015, proceedings, part III 18* (Springer, 2015), 234–241.
35. X. Chen, L. Yao, and Y. Zhang, "Residual Attention U-Net for Automated Multi-Class Segmentation of Covid-19 Chest CT Images," arXiv preprint, arXiv:2004.05645 (2020).
36. Z. Zhang, Q. Liu, and Y. Wang, "Road Extraction by Deep Residual U-Net," *IEEE Geoscience and Remote Sensing Letters* 15, no. 5 (2018): 749–753.
37. F. Isensee, P. F. Jaeger, S. A. Kohl, J. Petersen, and K. H. Maier-Hein, "NNU-Net: A Self-Configuring Method for Deep Learning-Based Biomedical Image Segmentation," *Nature Methods* 18, no. 2 (2021): 203–211.